

Sensor Network for Real-time In-situ Seismic Tomography

Lei Shi, Wen-Zhan Song, Fan Dong and Goutham Kamath

Georgia State University, Atlanta, Georgia, U.S.A.

Keywords: Sensor Networks, Design, In-network Processing and Seismic Tomography.

Abstract: Most existing seismic exploration or volcano monitoring systems employ expensive broadband seismometer as instrumentation. At present raw seismic data are typically collected at central observatories for post processing. With a high-fidelity sampling, it is virtually impossible to collect raw, real-time data from a large-scale dense sensor network due to severe limitations of energy and bandwidth at current, battery-powered sensor nodes. At some most threatening and active volcanoes, only tens of nodes are maintained. With a small network and post processing mechanism, existing system do not yet have the capability to recover physical dynamics with sufficient resolution in real-time. This limits our ability to understand earthquake zone or volcano dynamics. To obtain the seismic tomography in real-time and high resolution, a new sensor network system for real-time in-situ seismic tomography computation is proposed in this paper. The design of the sensor network consists of hardware, sensing and data processing components for automatic arrivaltime picking and tomography computation. This system design is evaluated both in lab environment for 3D tomography with real seismic data set and in outdoor field test for 2D surface tomography.

1 INTRODUCTION

In present, most existing seismic exploration or volcano monitoring systems use expensive broadband seismometer and collect raw seismic data for post processing. Seismic sampling rates for seismic exploration are usually in the range of 16-24 bit at 50-200Hz. Collecting all the raw data in real-time from a large-scale dense sensor network is virtually impossible due to severe limitations of energy and bandwidth at current, battery-powered sensor nodes. As a result, at some most threatening, active volcanoes, fewer than 20 nodes (Song et al., 2009) are thus maintained. With such a small network and post processing mechanism, existing system do not yet have the capability to recover physical dynamics with sufficient resolution in real-time. This limits our ability to understand earthquake zone or volcano dynamics and physical processes under ground or inside volcano conduit systems. Substantial scientific discoveries on the geology and physics of earthquake zone and active volcanism would be imminent if the seismic tomography inversion could be in real-time and the resolution could be increased by an order of magnitude or more. This requires a large-scale network with automatic in-network processing and computation capability.

To date, the sensor network technology has ma-

tured to the point where it is possible to deploy and maintain a large-scale network for volcano monitoring and utilize the computing power of each node for signal processing to avoid raw seismic data collection and support tomography inversion in real-time. The methods commonly used today in the procedure of seismic tomography computation cannot be directly employed under field circumstances proposed here because they rely on expensive broadband stations and post processing, also require massive amounts of raw seismic data collected on a central processing unit. Thus, real-time seismic tomography of high resolution requires a new mechanism with respect to low-cost energy efficient system design and in-network information processing. Then it is possible to deploy a large-scale network for long-term and compute the tomography in real-time. To clearly address the challenges in this paper, we first give a short description on the background knowledge of seismic tomography based on travelttime principle.

The first-arrival travelttime tomography uses P-wave first arrival times at sensor nodes to derive the internal velocity structure of the subsurface. The basic workflow of travelttime tomography illustrated in Figure 1 involves four steps: (a) P-wave Arrival Time Picking. Once an earthquake event happens, the sensor nodes that detect seismic disturbances record the signals. The P-wave arrival times need to be extracted

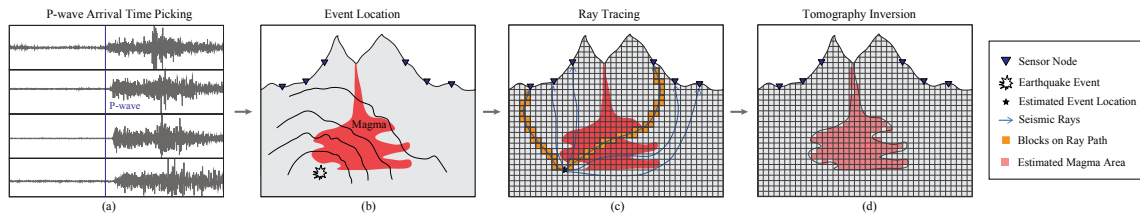


Figure 1: Workflow of first-arrival traveltimes tomography.

from the raw seismic data; (b) Event Location. The P-wave arrival times and locations of sensor nodes are used to estimate the event hypocenter and origin time in the volcanic edifice; (c) Ray Tracing. Following each event, seismic rays propagate to nodes and pass through anomalous media. These rays are perturbed and thus register anomalous residuals. Given the source locations of the seismic events and current velocity model, ray tracing is to find the ray paths from the event hypocenters to the nodes; (d) Tomography Inversion. The traced ray paths, in turn, are used to image a tomography model of the velocity structure. As shown in Figure 1 the volcano is partitioned into small blocks and the seismic tomography problem can be formulated as a large and sparse matrix inversion problem.

In traditional seismology, the raw seismic data is collected for manual analysis including P-wave arrival time picking on the seismograms. Then centralized methods will process the data and compute seismic tomography. Keep in mind that our goal is to design a system which can deliver tomography in real-time over a large-scale sensor network by utilizing the limited communication ability in the network and the computation power on the sensor node. To reach this goal, no raw seismic data should be transmitted over the network, which requires a light weighted algorithm that can accurately pick the P-wave arrival time on the sensor nodes locally inside the network.

This paper presents a sensor network system for real-time in-situ seismic tomography computation. The design of the sensor network consists of hardware, sensing, data processing, algorithm for automatic arrivaltime picking and so on. This system design is evaluated both in lab environment for 3D tomography with real seismic data set (previous deployment on San Andreas Fault (SAF) in Parkfield) and in outdoor field test for 2D surface tomography.

The rest of the paper is organized as follows. Section 2 shows the system architecture and discusses the system design in details. In section 3, we evaluate the signal quality compared with a industry level commercial data logger for seismology and validate the arrival time picking algorithm with both field test and real seismic data set. Section 4 describes the eval-

uation of the system both in lab environment and in outdoor field test. Section 5 discusses related work. Section 6 concludes this paper and outlines the future work.

2 SYSTEM DESIGN

In this section, we give the overview of our system architecture and the details of both hardware and software design. According to the motivation and requirement of the system design discussed above, the specific goals of the sensor network system design is as following:

- **Synchronized Sampling.** The event location and travel-time tomography requires the P-wave arrival time of earthquake events. The P-wave arrival time analysis is based on the temporal and spatial correlation of the recorded signals on stations. So all stations need to perform synchronized sampling and timestamp the record with precise UTC time. The synchronization accuracy should be less than the time interval of sampling (e.g. 20 millisecond for 50Hz sampling rate).
- **Long-term Robust Deployment.** To get accurate event location and high resolution seismic tomography, the more data recorded the better result can be potentially delivered. Since the earthquake activities are unpredictable, the long-term robust deployment is necessary to get enough data. Also, due to the harsh weather conditions for remote deployment, a low-cost energy efficient station with renewable energy and weatherproof capacity is required.
- **P-wave Arrival Time Picking.** As we discussed in section 1, this sensor network system will send the arrival time back instead of all raw seismic data. The system must be able to continuously monitor the signal, detect and pick arrival time in real-time.
- **Online Monitoring and Configuration.** To monitor the status of the network, perform the real-time signal processing and in-situ computation, the sensor network should be able to respond to

external control from the base station for status report or node configuration. The command and control needs to be delivered reliably in real-time.

- **Distributed Computation Extension.** This system is not limited to be a in-situ signal processing and data collection framework. In the future, the system can be used for more complicated seismic analysis that may include cross correlation of signals between stations, distributed computation and so on. Those tasks will require more computation power on each sensor node. An extension for adding a computation unit is required to make this system more extensive and general.

2.1 System Architecture

Our system consists of several components. Figure 2 shows the architecture of the sensor network system design. First, the sensor nodes with seismometers and RF modules form a mesh network. Each sensor continuously records the signal, once an event happened, the sensor will detect it and pick the P-wave arrival time from the signals. Then the arrival time along with the station coordinates is delivered to the base station. The base station is a computer that equipped with RF module, it runs various tools to process the received data, compute the tomography, visualize the result, monitor the network status and configure the sensor nodes. This system can deliver either 3D tomography through event location, ray tracing and inversion, or 2D surface tomography with Eikonal tomography method (Lin et al., 2009).

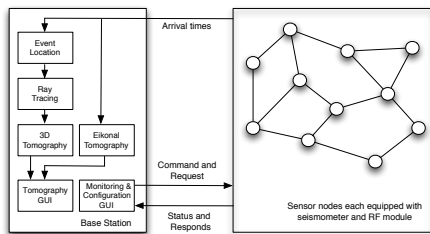


Figure 2: Sensor Network System Architecture.

2.2 Hardware Design

Considering the system design goals, our sensor node design encapsulates all the hardware components in a weatherproof plastic box. Figure 3 gives the configuration of the sensor node in the field. The sensor node box connected with a 10 Watt solar panel to get renewable energy. A single-axis 4.5Hz seismometer, GeoSpace geophone is connected as the sensor component. We mounted a 9 dBi omnidirectional antenna

on the box for the communication of a 900MHz RF module to get a reasonable line-of-sight range. All the connections are also sealed by weatherproof connectors for the harsh environment. The total weight of each sensor node station is about 10 pounds which can be carried by a person for remote deployment.



Figure 3: Sensor node in the field.

Figure 4 shows the hardware components inside the sensor node box, with a dimension of $0.82 \times 0.55 \times 0.31$ (inch). All our components in the system are mounted on a single-layer PCB board. The core of the system is a TI MSP430F6779 processor, 25MHz, 512KB of program ROM and 32KB of SRAM. This processor also provides seven independent 24-bit Sigma-Delta ADCs with different inputs and variable gain.

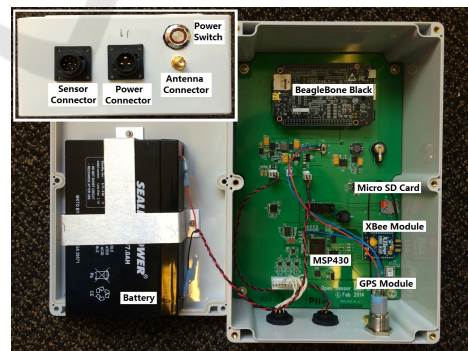


Figure 4: Hardware components in the box.

The low-power radionova M10478-A2 GPS interface is connected to the processor through UART1 to provide raw GPS data, and through GPIO 40 to provide PPS (pulse-per-second) signal capturing. The GPS interface is used to provide the coordinate of the sensor node and the timestamps for recorded data. For wireless communication, we employed the

XBee-PRO 900HP module to provide a low-power, low maintenance, long outdoor range and self organized wireless network. XBee module takes advantage of the DigiMesh networking protocol. It can run on dense network operation and support for sleeping routers for energy efficient. Besides, various point-to-multipoint configurations are available for the network. The MSP430 is connected to XBee using UART2 with 9600 baud that provides 960 Kbps data rate.

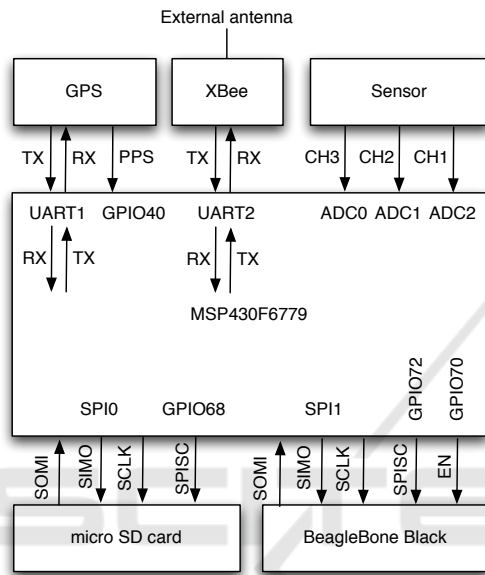


Figure 5: The main hardware components connection.

Since the sensor network is designed to sense the signal, pick and send the P-wave arrival timestamp back without transmitting the raw seismic data. All the raw data is stored in a micro SD card for other post analysis required by seismologists. We use the DM3D-SF connector and connect the processor with memory card through SPI0 for SPI communication and clock, and through GPIO 68 for SPI card select pin. The node sensor connector is designed to connect up to three channels of seismometer. The node can connect either to a single-axis or a tri-axis geophone. Both geophones are passive instruments and the ground motion can generate voltage which is digitized by the ADC module in MSP430.

For the distributed computation extension requirement, one BeagleBone Black (BBB) module is connected with the expansion connector to the board through its SPI0 interface. We use the SPI1 on MSP430 for SPI communication and clock, the GPIO 72 for SPI card select pin and the GPIO 70 as the power switch for BBB. The main hardware components connection relationships are shown in Figure 5.

2.3 Sensing and Data Processing

Aim to achieve the system design goals, based on our hardware design, we give the description of the software design for sensing and data processing on the sensor node in this section. Figure 6 illustrates the framework of the sensing and data processing components on the sensor node.

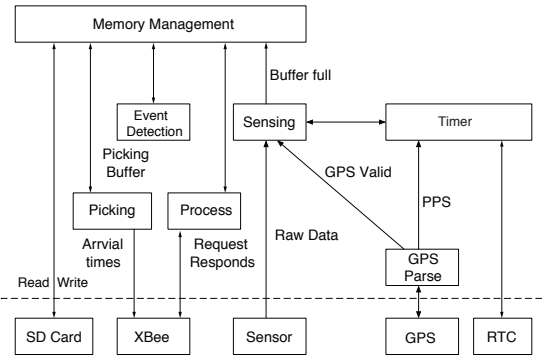


Figure 6: Sensing and Data Processing Framework.

Since the accurate event location and high-resolution tomography are depend on precise timing by utilizing the temporal and spacial correlation of recorded signals across stations. The first goal of our system design is synchronized sampling and precise UTC time timestamp for the recorded data. Our collaborators from seismology requires 100Hz sampling rate on our open nodes. Notice that, the synchronized sampling is based on time synchronization but not the same. Synchronized sampling does not only means that all sensor nodes in the network has the same sample interval but also sample at the same time point.

In the hardware design, each sensor node employs a low-cost GPS receiver that provides UTC time information and PPS signal. The GPS system time from GPS signal has an accuracy within 50ns referenced to UTC time, it can be used for time synchronization. The problem is that decoding and processing of the GPS message can generate delays and degrade the synchronization accuracy. Instead, we use PPS signals to synchronize the RTC. To achieve the synchronized sampling, we designed a *Timer* component to maintain RTC with millisecond resolution. Then when the system catches the first valid PPS interrupt, the timer is reset and keep counting on milliseconds. When next valid PPS interrupt is captured, if the timer is not in exact thousand milliseconds, the timer will be reset and the RTC will be synchronized properly.

Notice that, the GPS signal can disappear or the PPS signal can not fire properly. If the time period without GPS signal or valid PPS signals is long, the sampling across sensor nodes might not be synchro-

nized. The sensor node tags every second of data with a timestamp and a flag. The timestamp represents the time point corresponding to the first sample in this second. The flag indicates that whether the samples in this second is under valid time synchronization or not. The system will tag the second of data invalid synchronization if: (1) there is no GPS signal for 60 seconds; (2) there is no valid PPS interrupts for 20 seconds.

The *Sensing* component samples the sensor with 10 milliseconds sample interval according to the *Timer* component. There is a small circular buffer to sample one hundred samples (one second data under 100Hz) from sensor. Once this buffer is full. The *Sensing* component will send it to memory management to write the buffer into micro SD card with proper timestamp and flag. Also, the *Event Detection* component takes this buffer and perform the event detection processing, if one event is detected, the related buffered data is processed by *Picking* component to get the arrival time and send it through XBee module. Details about the event detection and arrival time picking are discussed in section 2.4. There is another module *Process* that processes the requests from base station and send responds back for status monitoring and network configuration. More details about this can be found in section 2.5.

2.4 P-wave Arrival Time Picking

Primary waves (P-waves) are the seismic waves that travel faster than any other waves through the earth. P-waves arrive at the seismic sensors first and the arrival time of P-waves are essential to the first-arrival traveltome tomography. Figure 7 shows the seismograms from two seismometers deployed in Parkfield when an event happens. The vertical lines represent manual pickings of the P-wave arrival times. Due to the different wave propagation delays, the P-wave arrival times on sensors are different. In local seismic tomography, the scale of the field is up to tens of kilometers and the maximum difference of the P-wave arrival times among sensors is about several seconds, so that the accuracy of the picking is significant. Besides, manual analysis of seismograms and picking of arrival times require post processing of the data and are very time consuming, especially in a large sensor network. To avoid raw seismic data transmission and meet the real-time requirements, the system demands an on-line automatic event detection and P-wave arrival time picking method that runs on each sensor node.

In this paper, we proposed a two-step method for P-wave arrival time picking. (1) Event Detection

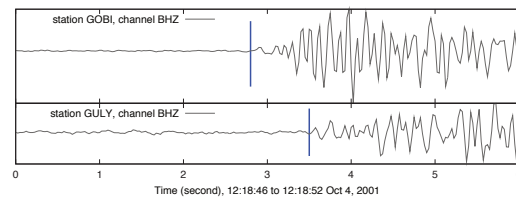


Figure 7: The seismogram from BHZ channel of two seismometers in Parkfield when an event happens. The vertical lines indicate the manual pickings of P-wave arrival times.

which continuously scanning the samplings from the sensor with a sliding window, claims if there is an event (change point) happens and extract a segment of signals around the change point; (2) Arrival Time Picking which takes the segment of signals from step (1), picks the exact change point (arrival time) from it and send the P-wave arrival time to coordinator node. Figure 8 illustrates how the proposed method works.

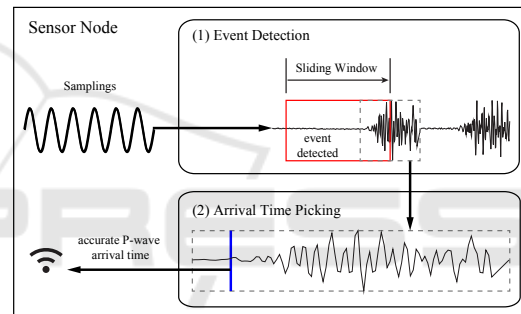


Figure 8: Two step P-wave arrival time picking.

In the first step, the goal is to continuously check whether there is a change point in the signal stream that is probably an event. The STA/LTA (short-term average over long-term average) algorithm (Murray and Endo, 1992; Song et al., 2009) is employed for event detection here because it is fast to monitor the signal and roughly find where an event happens. To describe STA/LTA algorithm, we need to first introduce the concept of RSAM (Realtime Seismic Amplitude Measurement), which is widely used in seismology. The RSAM is calculated on raw seismic data samples per second. Assume the sampling rate of the signal is m (samples per second), let $\{x_t, \dots, x_{t+m-1}\}$ and $\{x_{t-m}, \dots, x_{t-1}\}$ be the samples in the i -th and $(i-1)$ -th second respectively, then $e_{i-1} = \frac{\sum_{j=t-m}^{t-1} x_j}{m}$ is the average of the $(i-1)$ -th second. The i -th second RSAM r_i is calculated as $r_i = \frac{\sum_{j=t}^{t+m-1} (x_j - e_{i-1})}{m}$. In our system, the STA or LTA is continuously updated based on $X_i = \frac{\sum_{j=0}^{i-1} r_{i-j}}{n}$ where r_i is i -th second RSAM; n is the STA or LTA time window size (in seconds).

The ratio of STA over LTA is continuously moni-

tored. Once the ratio exceeds the threshold, an event is detected. A sliding LTA window with a STA window keep moving second by second and calculating the STA/LTA ratio. If the threshold b is reached, a change point is detected at T , the signal in the window of $[T - a, T + b]$ are extracted and the arrival time picking algorithm will pick the accurate arrival time from it. Then the sliding window continue moving from T and calculating the STA/LTA ratio, since the event usually lasts for a period of time, the STA/LTA ratio will be over the threshold for a while until time T' . In our implementation, the STA and LTA window are 1 and 4 seconds respectively; the signal window for picking is 3 seconds where $a = 1$ and $b = 2$. These parameters are all configurable in the network with base station. This setting with threshold 2 can perform event detection very well for picking as shown in section 3.2. Figure 9 gives an example of event detection result and the detection length of a real earthquake event.

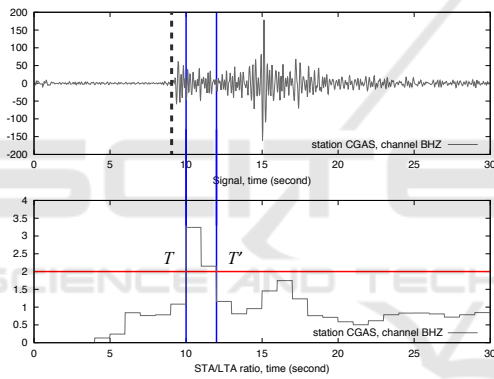


Figure 9: Event detection example on a real earthquake event.

From the seismograms in Figure 7, one can see that there is a big difference on the amplitude variance of the signal before and after the arrival of P-waves, the P-wave arrival time is a change point of the variance of the signal amplitude. Based on this observation, a P-wave picking method in step two is proposed in this paper by utilizing the maximum-likelihood (ML) estimation to estimate the variance of the signal amplitude following a statistical model.

Without loss of generality, we assume that both the pre- and post-change (before and after P-wave arrival) signals follow a normal distribution but with different variances. Let $\{x_i\}_{i=1}^t$ be the continuous sequence of samples from 1 to t , then the pre- and post-change sample has a normal distribution with zero mean respectively. Then the pre-change sample $x_i \sim \mathcal{N}(0, \sigma_1^2)$ and the post-change sample $x_i \sim \mathcal{N}(0, \sigma_2^2)$. The logarithm of the likelihood function at time k

can be written as $\mathcal{L} = \sum_{i=k+1}^t \left[\frac{1}{2} \ln \frac{\sigma_1^2}{\sigma_2^2} - \frac{x_i^2}{2} \left(\frac{1}{\sigma_2^2} - \frac{1}{\sigma_1^2} \right) \right]$. The arrival time picking is to find the exact change point k^* in $[T - a, T + b]$ which maximize the function value of \mathcal{L} . Due to the length limit, we omit the full mathematical derivation process and equations for the P-wave picking calculation.

2.5 Online Monitoring and Configuration

Considering the complexity and remoteness of environment monitoring, online status monitoring and sensor node configuration are highly desired. With online monitoring, users can easily get the status of the sensor nodes in the network. This is very helpful when the deployment is initiating, one can monitor all the sensor nodes in the network remotely without actually visiting them remotely. There are two modes in the system, test and deploy. When the deployment starts, the node will start with test mode, and it will report the status periodically. After a while, if the node status is normal, users can switch the nodes to deploy mode where the sensor node only report the status if requested. The status report consists of the GPS status (satellite numbers, latitude, longitude, altitude), the sensing status (number of events detected, number of seconds recorded), the power status (solar panel input voltage and battery voltage). Besides, many parameters need to be configurable in the sensor node. For example, the window size and threshold in the event detection and picking algorithms. Since different kind of events have different properties, different parameters could identify various classes of events according the interesting of seismologists. Also, the sensing parameters such as channel, data resolution, sensor status and reference voltage gain can also be configured.

In our system design, the sensor node only sends the arrival time with station information back by default. One problem is that in different field or with different interests for events, the parameters for event detection and picking can be varied. After deployment, users need to know whether the arrival time picking is accurate or not. Thus, a stream option is added into the system. When the stream option is on, the sensor node will send the raw stream data in the picking buffer with the arrival time. Users can visualize it on base station to check the picking accuracy on base station in real-time. Figure 10 shows the stream data and arrival time picking from the monitoring and configuration tool on the base station. Besides, seismologists might be interesting in the raw data for other analysis in the deployment period. Then can not afford to visit the sensor node remotely all the time. Another feature in this system is that users can download the data

from a any node by specifying the start and end time point.

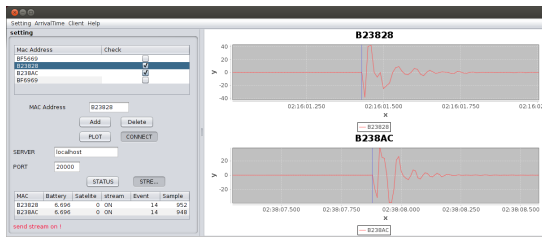


Figure 10: Stream data with arrival time picking.

3 DATA QUALITY AND PICKING ACCURACY

Before the field deployment and end-to-end tomography computation test of the system, we conducted several tests to verify the quality of recorded data with the sensor node and the accuracy of the arrival time picking mechanism.

3.1 Data Quality

The scientific value of the data is the final and most important measurement of the sensor network system. The first test here is to see weather this system can provide scientifically meaningful data to seismologists. Since it is not easy to find a place to record earthquake events and it might take long time to validate. With the suggestion from seismologists, we conduct a hammer shock test that is commonly used by the experts for preliminary. This test is to use a hammer to hit on the ground to generate seismic wave propagation. The signal from a hammer shock is not so different from an earthquake except the energy is smaller.



Figure 11: SigmaBox configuration.

To validate the data quality, the test is conducted to compare the data recorded by our sensor node and

a current state of the art commercial seismic acquisition system called SigmaBox. The SigmaBox is designed by iSeis Corporation¹, shown in Figure 11. In the test, 7 sensor nodes and 4 SigmaBox are deployed. Four sensor nodes are placed with SigmaBoxes side by side to compare the recorded data quality, see Figure 12. The distance between each pair of nodes is 10 meters. We used the hammer to hit the ground near the SigmaBox 70 and sensor node 18 for 20 times. In Figure 13, we can see the recorded data for a hammer shock event by our sensor node and SigmaBox. The SNR is similar between two data record and the seismologist were satisfied with the data quality overall.



Figure 12: SigmaBox and sensor node deployment.

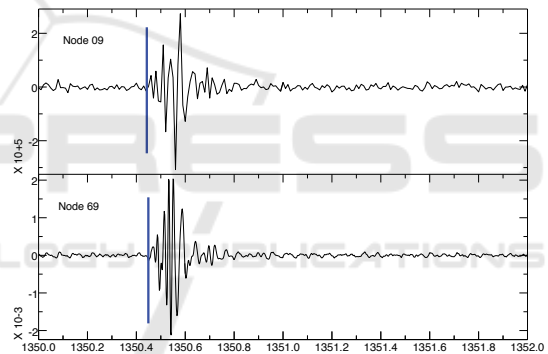


Figure 13: Waveform of a hammer shock event on sensor node 09 and SigmaBox 69.

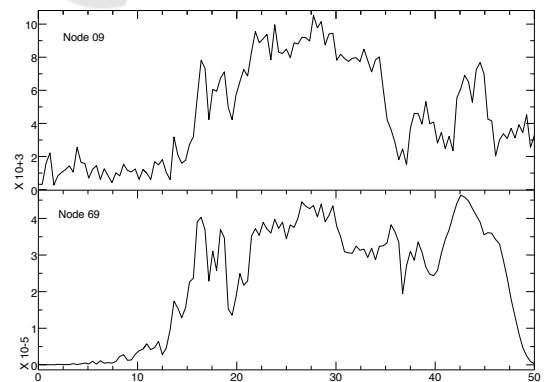


Figure 14: Spectrum of the hammer shock event on sensor node 09 and SigmaBox 69.

The spectrum of the waveform in Figure 13 is

¹<http://www.iseis.com>

shown in Figure 14. We can see that the spectrum distribution is similar between two signals. This further validate the data quality of our sensor node. Notice that the SigmaBox costs about \$3K, while the sensor node costs less than \$1K.

3.2 P-wave Arrival Time Picking Accuracy

The example in Figure 13 shows the arrival time picking of our algorithm on sensor node and SigmaBox sensed data. Notice that the sampling rate of SigmaBox was 500Hz in the test. In the example, the time difference between two pickings is 6 millisecond, which is smaller than the sampling interval of our sensor node. The average time difference of all pair of pickings in this test is 4.2 millisecond. This test shows that the algorithm can deliver similar arrival time result on different node. But it only means that the recorded data quality from two kinds of nodes is similar to perform detection and picking algorithm. To validate the accuracy of the picking algorithm, the algorithm should perform on the real data set with manual pickings from experts as the reference.



Figure 15: Audio to sensor channel adapter.

We used a real data set obtained from seismologists. This data set was recorded from a previous deployment on San Andreas Fault (SAF) at Parkfield. The deployment is from Jan 1, 2000 to Dec 31, 2002 with 61 stations. The data set has been cut into short waveforms that contain events with the manual pickings. Then the problem is that how can we send the waveforms to sensor node for validation. We made an adapter from audio input to channel 0 as shown in Figure 15. Then waveforms were converted into audio wave and can be sent to the sensor node by any audio player on a computer, cellphone or tablet. There are totally 4478 arrival times picked by the algorithm from the data set. About 91% picking errors of our algorithm are within 0.2 seconds. The mean value and the standard deviation of the difference between

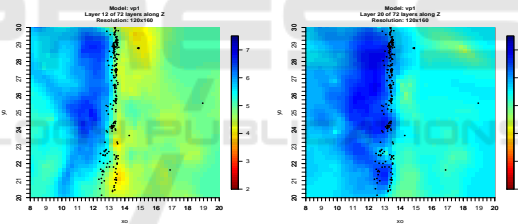
our pickings and manual pickings are 0.043 and 0.23. This is comparable with some recent method in seismology literature (Zhang et al., 2003).

4 SYSTEM EVALUATION

In this section, we conduct two experiments to evaluate the sensor network system for both 3D and 2D surface tomography.

4.1 Parkfield 3D Tomography

From the discussion of previous section, we use an adapter to send the waveform from computer to our sensor nodes simulating the sampling process. The sensor node then process the data, picked the arrival times and send to a base station set in the lab. After the base station received some arrival times, it should compute the event location. Notice that this computation is an online process, because in real deployment, one can not predict when and how many arrival times can be received since the earthquake activity is not predictable.



(a) V_p at depth = 2km (b) V_p at depth = 4km

Figure 16: Horizontal slices of the P-wave velocity at depths of 2, 4 km. The fault is located around $X=13.5$ km.

The base station only receives the arrival times from the sensor nodes and has the knowledge that which picking is from which node. In all of these pickings, there might be false alarms or some small and remote event is only detected by few sensor nodes. As we known, to estimate an event location and origin time, at least four pickings from different sensor nodes are required, the event detected only by one or two nodes is impossible to be located. Also, more pickings from different sensor nodes for one event usually lead to a better estimation. Thus there are two steps in event location, (1) Event Identification where the base station identifies how many events existing in a series of arrival times received and which pickings belong to the same event; (2) Location Estimation which uses Geiger's method to estimate the event location from the arrival times of that event.

After identified the events and computed the event locations, base station will do ray tracing based on the event information and the station coordinates received with the arrival times, followed by the 3D tomography inversion.

Figure 16 shows the tomography result from the base station. It is easy to see that the velocity model is different on different side of SAF. The dots in the tomography indicate the event locations estimated on base station. A scientific fact is that the events often happen around the fault which is verified by our result. We can see that the fault feature is easy to get from the tomography result. This result is comparable with the previous research on the Parkfield tomography (Zhang et al., 2009).

4.2 Hammer Shock Field Test

To verify the sensor network system in outdoor field, we conduct a field test and created the event with hammer shock on the ground to generate the surface wave. In this case, we can control the location of the event source and it is easy to verify if the recorded data is meaningful, the arrival time pickings is correct and the 2D surface tomography result is validated.



Figure 17: Hammer shock test deployment.

In the previous discussion, the hammer shock test has already been used for data quality and arrival time picking validation. From that test, we found that on the soil ground, the hammer shock can generate waves propagated up to around 30 meters, depends on how hard the hammer hit the ground. Thus, 25 sensor nodes are deployed on a 20 × 20 meter area with 5 meter space between the adjacent sensor nodes. Figure 17 shows the deployment of 25 sensor nodes. In the area we deployed, the upper half of it covered by wet soil under the tree while the other half is covered by drier soil under the sunshine in day time. The reason we choose this area is that we would like to see the difference from Eikonal tomography based on the property of the different acoustic wave propagation speed in wet and dry soil.

After the deployment done, the base station monitored the status of all sensor nodes and told us when all nodes started working normally. Then we created

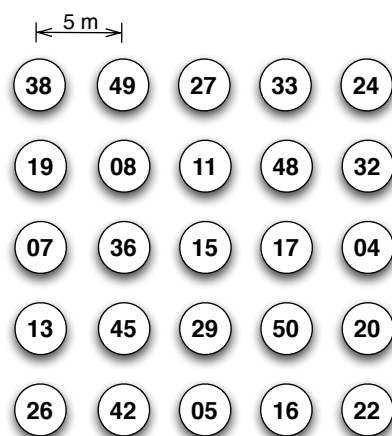


Figure 18: Deployment map of sensor nodes.

5 hammer shocks (events) beside each station, totally 125 events were created. The deployment map of the sensor nodes is shown in Figure 18.

Finally, after all hammer shocks done, the base station received more than 2000 arrival times and computed the 2D surface tomography with Eikonal tomography method. Before showing the tomography result, we take a closer look at one seismic event recorded by the sensor network and the arrival times picked out of this event.

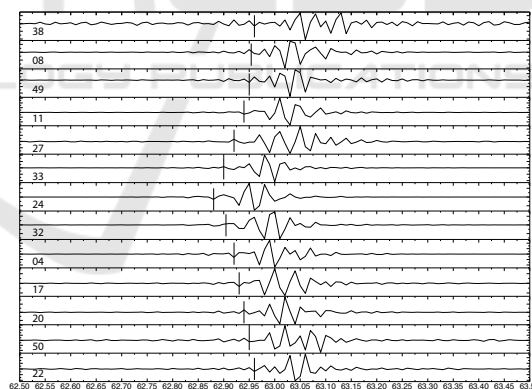


Figure 19: Hammer shock event captured.

The hammer shock event captured in Figure 19 was generated by hit beside node 24, which located on the upper right corner in the deployment map. From the recorded signal and picked arrival times shown in Figure 19, node 24 got the earliest arrival time and the further nodes got the relatively delayed arrivals, which shows the wave propagation in the deployed area. Within such a small area, this further verified the synchronized sampling accuracy of our sensor network system.

In this test, the base station received totally 2012 arrival times picked on the sensor nodes. Some events

are not picked on some nodes. The reason is that the sensor node can not get good event signal, it depends on how hard the hammer hit the ground and how far the sensor node is from the event location.

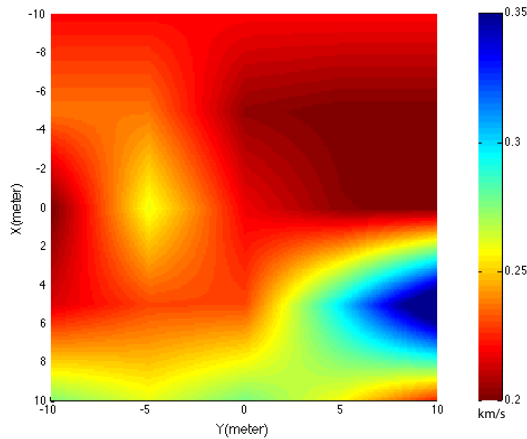


Figure 20: 2D surface wave tomography.

Out of 2012 arrival times, the base station identified 96 events with 1905 arrival times. Figure 20 shows the 2D surface wave tomography delivered by the base station. According to the research on acoustic wave propagation in soil (Oelze et al., 2002), the impedance mismatch from the water to air is much greater than the water to soil frame. Thus, more saturated the soil is, slower the acoustic wave propagates in it. As we discussed above, the upper side of the deployed area contains more water in the soil. This observation is shown in the final tomography result.

5 RELATED WORK

Static tomography inversion for 3D structure, applied to volcanoes and oil field explorations, has been explored since the late 1970's (Iyer and Dawson, 1993; Vesnaver et al., 2003; Lees, 2007). In volcano applications, tomography inversion used passive seismic data from networks consisting of tens of nodes, at most. The development and application to volcanoes include Mount St. Helens (Lees, 1992; Lees and Crosson, 1989; Waite and Moranb, 2009), Mt. Rainier (Moran et al., 1999), Kliuchevskoi, Kamchatka, Russia (Lees et al., 2007), and Unzen Volcano, Japan (Ohmi and Lees, 1995). At the Coso geothermal field, California, researchers have made significant contributions to seismic imaging by coordinating tomography inversions of velocity (Wu and Lees, 1999), anisotropy (Lees and Wu, 1999), attenuation (Wu and Lees, 1996) and porosity (Lees and Wu, 2000).

Sensor network has been deployed for monitoring in many different areas. In (Cerpa et al., 2001), the sensor network was deployed to collect dense environmental and ecological data about populations of rare species and their habitats. Another sensor system was used by the researchers to monitor the habitat of the Leach's Storm Petrel at Great Duck Island (Szewczyk et al., 2004). The Zebranet (Juang et al., 2002) project uses sensor network nodes attached to zebras to monitor their movements via GPS. It is composed of multiple mobile nodes and a base station with occasional radio contact. The sensor network was also used to monitor the bridge health (Kim et al., 2006; Chebrolu et al., 2008) and weather condition as well (Hartung et al., 2006).

For volcano monitoring, The first volcanic monitoring work using WSN was developed in July 2004 (Werner-Allen et al., 2006), by a group of researchers from the Universities of Harvard, New Hampshire, North Carolina, and the Geophysical Institute of the National Polytechnic School at Reventador in Ecuador. Data collection was performed with continuous monitoring during 19 days.

In 2008, a smart solution was proposed for collecting reliable information aiming to improve the collection of real-time information. The sensor network was deployed on Mount St. Helens (Song et al., 2009) for volcano hazard monitoring and run for months.

6 CONCLUSION

In this paper we presented a sensor network system that performs in-situ signal processing and obtained 3D or 2D surface tomography in real-time. The hardware and software design of the system focused on delivering a low-cost, energy efficient and reliable system to monitor and image the earthquake zone or active volcano. Several tests and experiments were conducted to show: (1) the recorded data quality is similar to current commercial industry level product; (2) the system can deliver the validated tomography result. This sensor network system marks the collaboration between geophysicists and computer scientists that provided opportunities to introduce new technology for geophysical monitoring. The design and presented here has broader implication beyond tomography inversion and can be extended to oil and natural gas exploration.

Our future plan is to deploy a larger scale sensor network on a real volcano for a long-term run, and further verify the correctness, the efficiency and the robustness of the system. Another plan in the future involves the development of distributed algorithm to

compute the tomography in a fully distributed manner without a base station by utilizing the extension of the computation unit in the sensor node.

REFERENCES

- Cerpa, A., Elson, J., Estrin, D., Girod, L., Hamilton, M., and Zhao, J. (2001). Habitat Monitoring: Application Driver for Wireless Communications Technology. In *1st ACM SIGCOMM Workshop on data communication in Latin America and the Caribbean*.
- Chebroly, K., Raman, B., Mishra, N., Valiveti, P. K., and Kumar, R. (2008). BriMon: A Sensor Network System for Railway Bridge Monitoring. In *The 6th Annual International Conference on Mobile Systems, Applications and Services (MobiSys)*.
- Hartung, C., Han, R., Seielstad, C., and Holbrook, S. (2006). FireWxNet: A Multi-Tiered Portable Wireless System for Monitoring Weather Conditions in Wildland Fire Environments. In *The 4th International Conference on Mobile Systems, Applications, and Services (MobiSys 2006)*.
- Iyer, H. M. and Dawson, P. B. (1993). *Imaging volcanoes using teleseismic tomography*. Chapman and Hall.
- Juang, P., Oki, H., Wang, Y., Martonosi, M., Peh, L., and Rubenstein, D. (2002). Energy Efficient Computing for Wildlife Tracking: Design Tradeoffs and Early Experiences with ZebraNet. *Proc. 10th international conference on Architectural support for programming languages and operating systems*.
- Kim, S., Pakzad, S., Culler, D., Demmel, J., Fenves, G., Glaser, S., and Turon, M. (2006). Wireless sensor networks for structural health monitoring. In *Proc. 4th ACM conference on Embedded networked sensor systems (SenSys)*.
- Lees, J. M. (1992). The magma system of Mount St. Helens: non-linear high-resolution P-wave tomography. *Journal of Volcanology and Geothermal Research*, 53:103–116.
- Lees, J. M. (2007). Seismic tomography of magmatic systems. *Journal of Volcanology and Geothermal Research*, 167(1-4):37–56.
- Lees, J. M. and Crosson, R. S. (1989). Tomographic Inversion for Three-Dimensional Velocity Structure at Mount St. Helens Using Earthquake Data. *Journal of Geophysical Research*, 94(B5):5716–5728.
- Lees, J. M., Symons, N., Chubarova, O., Gorelchik, V., and Ozerov, A. (2007). Tomographic images of klichhevskoi volcano p-wave velocity. *AGU Monograph*, 172:293–302.
- Lees, J. M. and Wu, H. (1999). P wave anisotropy, stress, and crack distribution at Coso geothermal field, California. *Journal of Geophysical Research*, 104(B8):17955–17973.
- Lees, J. M. and Wu, H. (2000). Poisson's ratio and porosity at Coso geothermal area, California. *Journal of Volcanology and Geothermal Research*, 95(1-4):157–173.
- Lin, F.-C., Ritzwoller, M. H., and Snieder, R. (2009). Eikonal tomography: surface wave tomography by phase front tracking across a regional broad-band seismic array. *Geophysical Journal International*, 177(3):1091–1110.
- Moran, S. C., Lees, J. M., and Malone, S. D. (1999). P wave crustal velocity structure in the greater Mount Rainier area from local earthquake tomography. *Journal of Geophysical Research*, 104(B5):10775–10786.
- Murray, T. L. and Endo, E. T. (1992). A real-time seismic-amplitude measurement system (rsam). volume 1966 of *USGS Bulletin*, pages 5–10.
- Oelze, M. L., O'Brien, W. D., and Darmody, R. G. (2002). Measurement of attenuation and speed of sound in soils. *Soil Science Society of America Journal*, 66(3):788–796.
- Ohmi, S. and Lees, J. M. (1995). Three-dimensional P- and S-wave velocity structure below Unzen volcano. *Journal of Volcanology and Geothermal Research*, 65(1-2):1–26.
- Song, W.-Z., Huang, R., Xu, M., Ma, A., Shirazi, B., and Lahusen, R. (2009). Air-dropped Sensor Network for Real-time High-fidelity Volcano Monitoring. In *The 7th Annual International Conference on Mobile Systems, Applications and Services (MobiSys)*.
- Szewczyk, R., Polastre, J., Mainwaring, A., Anderson, J., and Culler, D. (2004). Analysis of a Large Scale Habitat Monitoring Application. In *Proc. 2nd ACM Conference on Embedded Networked Sensor Systems (SenSys)*.
- Vesnaver, A. L., Accaino, F., Bohm, G., Madrussani, G., Pajchel, J., Rossi, G., and Moro, G. D. (2003). Time-lapse tomography. *Geophysics*, 68(3):815–823.
- Waite, G. P. and Moran, S. C. (2009). VP Structure of Mount St. Helens, Washington, USA, imaged with local earthquake tomography. *Journal of Volcanology and Geothermal Research*, 182(1-2):113–122.
- Werner-Allen, G., Lorincz, K., Johnson, J., Lees, J., and Welsh, M. (2006). Fidelity and Yield in a Volcano Monitoring Sensor Network. In *Proc. 7th USENIX Symposium on Operating Systems Design and Implementation (OSDI)*.
- Wu, H. and Lees, J. M. (1996). Attenuation structure of Coso geothermal area, California, from wave pulse widths. *Bulletin of the Seismological Society of America*, 86(5):1574–1590.
- Wu, H. and Lees, J. M. (1999). Three-dimensional P and S wave velocity structures of the Coso Geothermal Area, California, from microseismic travel time data. *Journal of Geophysical Research*, 104(B6):13217–13233.
- Zhang, H., Thurber, C., and Bedrosian, P. (2009). Joint inversion for Vp, Vs, and Vp/Vs at SAFOD, Parkfield, California. *Geochem. Geophys. Geosyst.*, 10(11):Q11002+.
- Zhang, H., Thurber, C., and Rowe, C. (2003). Automatic P-Wave Arrival Detection and Picking with Multiscale Wavelet Analysis for Single-Component Recordings. *Bulletin of the Seismological Society of America*, 93(5):1904–1912.